Magnetoresistance Crossover in Cobalt/Poly(3-hexylthiophene,2,5-diyl) Hybrid Films Due to the Interface Effect

Lingcheng Zheng,[1] Jie He,[1] Deqiang Feng,[1] Rui Zhang,[1] Hui Liu,[2] Xinghua Zhang,[3] Zunming Lu,[3] Weichao Wang,[1] Wei-Hua Wang,[1] Feng Lu,[1] Hong Dong,[1] Yahui Cheng,[1,4,*] Luyan Li,[5] Rongkun Zheng,[4,†] and Hui Liu[1]

[1]*Department of Electronics and Key Laboratory of Photo-Electronic Thin Film Devices and Technology of Tianjin, Nankai University, Tianjin 300350, China*
[2]*Research Group of Quantum-Dot Materials & Devices, Institute of New-Energy Materials, Tianjin University, Tianjin 300350, China*
[3]*School of Material Science and Engineering, Hebei University of Technology, Tianjin 300130, China*
[4]*School of Physics, The University of Sydney, NSW 2006, Australia*
[5]*School of Science, Shandong Jianzhu University, Jinan 250101, China*

Cobalt/poly(3-hexylthiophene,2,5-diyl) (Co/P3HT) hybrid films with different Co thicknesses are prepared by magnetron sputtering combined with solution process. An anomalous magnetoresistance (MR) crossover phenomenon changing from the intrinsic negative sign of Co to positive with decreased Co thickness is observed. The electric transport measurement indicates that the weak localization (WL) effect gradually dominants the Co/P3HT at low temperature with decreased Co thickness. The MR test in different magnetic-field directions reveals the MR crossover phenomenon that results from the Co/P3HT contact due to the Co penetration and the formation of the reverse barrier. These results show the significant influence of the metal/organic semiconductor interface on the MR effect.

I. INTRODUCTION

In recent years, organic semiconductors (OSCs) have been intensively studied for applications in sensors [1], light-emitting diodes [2], field-effect transistors [3], solar cells [4], artificial photosynthesis [5], and so on, due to their good properties, low cost, flexibility, and large-scale manufacturing. Compared with their inorganic counterparts, OSCs possess long spin-diffusion lengths because of the weak spin-orbit coupling (SOC) and hyperfine interaction. In 2002, Dediu *et al.* first applied OSCs into spin valves (SVs), which opened the field of organic spintronics [6]. Recently, Sun *et al.* fabricated a molecular spin-photovoltaic device that integrates a photovoltaic response with the spin transport across the molecular layer [7]. This work presented deeper insight about the OSCs' potential in multifunctional applications.

At present, the magnetoresistance (MR) effect has been widely studied and commercialized [8]. However, the value of MR still needs to be further improved for wider practical applications, and the physical mechanism needs to be better understood. In particular, the MR effect in metal/OSC hybrid materials and devices is complicated

due to serious problems such as interdiffusion and metal inclusions in metal/organic contacts, which will cause an ill-defined interface layer [9]. Many investigations have indicated that the metal/OSC ill-defined interface layer significantly influences MR performance. Barraud *et al.* proposed that the spin-hybridization-induced polarized states at the interface can improve or inverse MR [10]. Ciudad *et al.* reported that a chemically engineered interface can help to control the sign of the MR [11]. Mandal's calculation showed that a small change of approximately 3% in the metal molecule interfacial distance could alter the sign of MR in a molecular SV device [12]. Recently, Ding *et al.* found that the inversed MR in P3HT-based SV results from the penetration of a Co electrode [13]. Obviously, although the roles of metal/OSC interface are important, the physical mechanisms are still controversial.

Because the metal/OSC interface effect in organic spin valves (OSVs) is significant, it is necessary to study the transport properties of the interface layer separately to reveal its contribution to OSVs. However, research on the individual interface layer is still rather rare. In this work, we design a poly(3-hexylthiophene,2,5-diyl) (P3HT) film covered by a very thin layer of Co to simulate a metal/OSC interface layer. We aim to extract the interface layer and study its MR. To achieve this, we use the same magnetron sputtering technology as the top electrode of the OSV, but

*chengyahui@nankai.edu.cn
†rongkun.zheng@sydney.edu.au

only shorten the sputtering time. In the very short depositing time, most of the Co penetrates into P3HT due to its soft texture, forming a metal/organic semiconductor hybrid layer instead of a continuous top electrode layer. The hybrid layer in this work is consistent with the interface layer in OSV. The interface effects of Co/P3HT are investigated via electric and magnetic transport measurements.

Co is a commonly used ferromagnetic contact in organic spintronic devices and P3HT, as a typical π-conjugated polymeric OSC, possesses a longer conjugation length and fewer intrinsic defects than do small molecules. The spin diffusion length of P3HT is 80 nm, which is much higher than that of inorganic semiconductors [14]. All these advantages make P3HT a promising material for applications in organic spintronics or for studying the basic physics, such as the Hall effect [15], MR effect [16], and metal/organic contact effect [17]. Our results reveal that the interface effect inverses the MR from negative to positive in Co/P3HT hybrid films and a model is proposed to explain the observations.

II. EXPERIMENTAL DETAILS

Co/P3HT hybrid films are prepared as follows. Ten mg/ml P3HT ortho-dichlorobenzene (ODCB) solution is filtered with a 0.45-μm filter and then spin-coated on a cleaned glass substrate with a spin speed of 2000 r/min. The coated P3HT film is annealed for 10 min at 120 °C in vacuum. The average P3HT thickness is determined to be 20 nm using a scanning electron microscope (SEM, S-3500N). Co (99.99%) is sputtered on the annealed P3HT films through a shadow mask via dc magnetron sputtering. The base pressure of the chamber before deposition is lower than 1×10^{-4} Pa. Sputtering power and Ar pressure are kept at 45 W and 0.5 Pa, respectively. The deposition rate of Co is determined to be approximately 5 nm/min by cross-section SEM. A series of Co films are deposited on the annealed P3HT films and directly on glass substrates for comparison. These samples are named according to the nominal Co thickness x (nm) as Co_x/P3HT or Co_x, where the thickness x is 10, 12.5, 15, 17.5, 25, and 50, respectively.

Microstructures are characterized by transmission electron microscopy (TEM, JEOL 2200F) operating at 200 kV. Resistance, magnetoresistance, and Hall resistance measurements are carried out via a four-probe dc technique using a physical properties measurement system (Quantum Design PPMS-9) in a magnetic field of up to 5 T. The sample photos and the conductive circuit are illustrated in Fig. S1 (see Supplemental Material [18]).

III. RESULTS AND DISCUSSION

TEM bright-field images and the selected area electron diffraction (SAED) patterns of Co_10 and Co_10/P3HT samples are presented in Figs. 1(a) and 1(b), revealing the
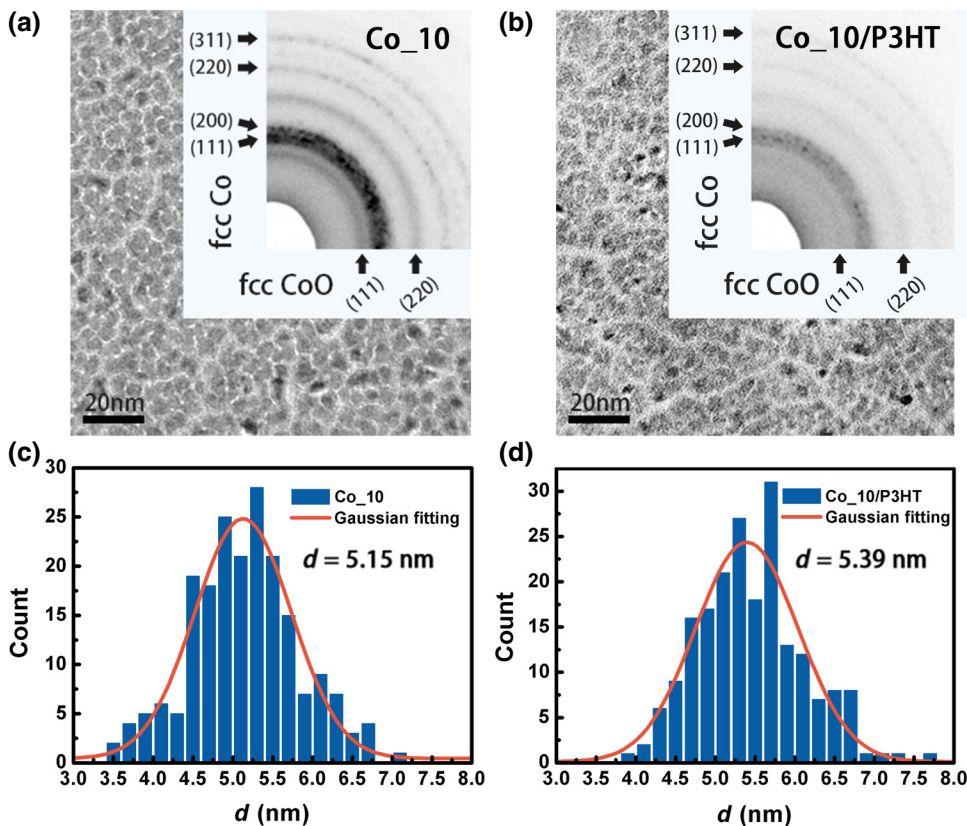

FIG. 1. TEM bright-field images and SAED patterns of (a) Co_10 and (b) Co_10/P3HT. (c),(d) are the particle size histograms (bars) and Gaussian fitting curves (solid line) for Co_10 and Co_10/P3HT.

granular nature of the films. Figures 1(c) and 1(d) are the particle size statistics of over 200 particles for the Co_10 and Co_10/P3HT from the TEM images. The average particle sizes d are 5.15 and 5.39 nm, respectively, for Co_10 and Co_10/P3HT, which are obtained by the Gaussian fitting. Diffraction rings in the insets of Figs. 1(a) and 1(b) indicate that both of the films are polycrystalline. The labels of (311), (220), (200), and (111) planes on the left correspond to the fcc Co phase, while the labels of (111) and (220) planes on the bottom correspond to the fcc CoO phase, indicating that the sputtered Co films are slightly oxidized in the ambient. These results imply that P3HT has little influence on the morphology and microstructure of the Co films.

The longitudinal resistivity vs temperature curves (ρ–$\log T$) of the Co_10 and Co_50 samples are presented in Fig. 2(a). The Co_50 film displays a positive temperature coefficient of resistivity (TCR), that is, a bulk transport behavior. In contrast, the Co_10 film displays a resistivity 20 times larger than that of the Co_50 film, and a negative TCR emerges in the ρ–$\log T$ curve below the critical temperature $T_{\min}$ of 83 K, which is the temperature corresponding to the residual resistivity [19]. The good linear dependence of ρ on $\log T$ below $T_{\min}$ indicates the existence of the weak localization (WL) effect [20]. That is, in these highly disordered granular Co films (shown in Fig. 1), a large number of granule boundaries as well as the surface oxidation significantly scatter the conduction electrons, lead to the localization of conduction electrons, and induce an increased resistivity and ρ–$\log T$ dependence at low temperature. The magneto-transport results will also support the existence of WL, which will be discussed in the following section. Note that the $\log \rho \propto T^n$ relation is not observed at low temperature and the resistivity does not change much, thus the tunneling effect

does not occur in this situation. Therefore, it is believed that the CoO phase displays surface oxidation in ambient instead of granular oxidation during deposition. The previous work by Brands *et al.* showed that if 10-nm Co film was capped by 2-nm Pt film as a protective layer to avoid oxidation [21], the WL effect was not observed, which is much different from the nature of the bare Co_10 sample in our experiment. Meanwhile, in the quasi-two-dimensional CoO-coated Co-cluster assemblies, similar electric transport behavior caused by WL is observed due to the slightly oxidized Co [20]. Therefore, it can be inferred that in this work, the CoO phase is responsible for the observed significant increase of resistivity at low temperature, that is, the WL effect of the Co_10 film. In contrast, no resistivity enhancement is observed at low temperature in the Co_50 sample, which may be because the oxidation of Co has a much weaker influence on the bulk electric transport of the Co_50 sample.

The ρ–$\log T$ curve of the Co_10/P3HT sample is also shown in Fig. 2(a). Resistivity of the Co_10/P3HT sample is much lower than that of the bare Co_10 sample, and the $T_{\min}$ of the Co_10/P3HT sample is 52 K, also lower than that of the Co_10 sample. These features indicate an improved electric conductivity. It is known that at each metal/OSCs contact area, the charge transfer will lead to a tilt of the energy level. In the case of different relative Fermi level positions of metal and OSCs, the charge transfer results in charge depletion or accumulation, forming the "Schottky barrier" or "reverse barrier" [22,23]. As shown in Fig. 2(b), the work function of Co is −5.0 eV, and the HOMO level of P3HT is −4.92 eV (This value was collected by electrochemical Mott-Schottky test [24], see Supplemental Material [18].). As a result, the electrons in P3HT flow toward Co and cause the energy level of P3HT to lift around the interface. Electrons flow away,
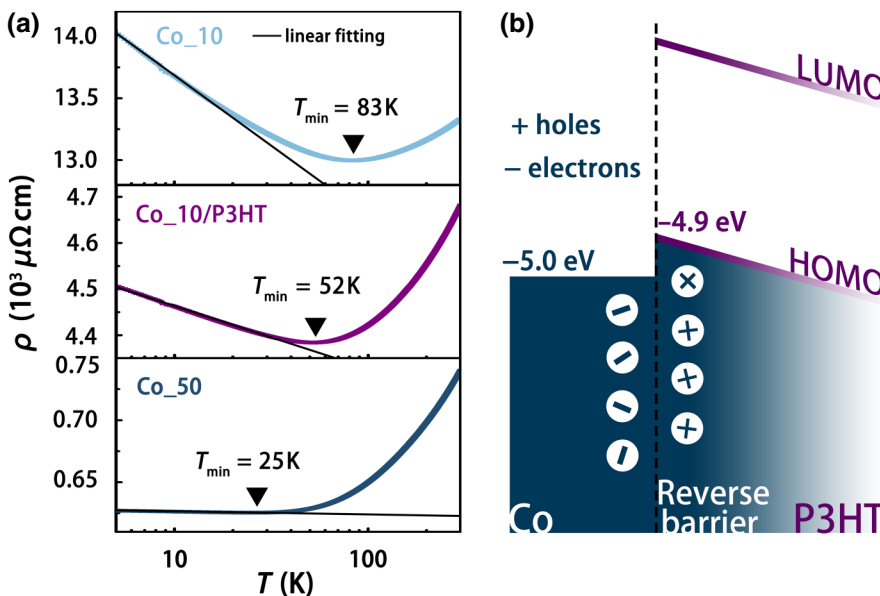

FIG. 2. (a) The ρ–$\log T$ curves of Co_50, Co_10/P3HT, and Co_10, respectively. (b) The schematic diagram of energy-level structure of Co/P3HT.
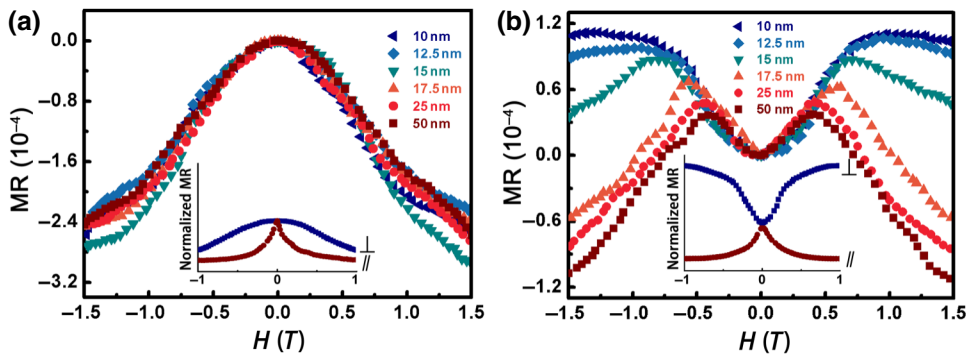
FIG. 3. MR vs magnetic field curves of (a) Co_x and (b) Co_x/P3HT samples with different film thicknesses at RT. The insets of (a),(b) are the MR curves of Co_10 and Co_10/P3HT samples with a magnetic field perpendicular to the film and parallel to the electric current direction, respectively.

leaving a large number of majority carriers (holes) accumulating in P3HT close to the Co/P3HT interface, forming the ultrathin so-called reverse barrier with high conductivity [25]. Moreover, it has been widely reported that in the metal/OSC hybrid films, the metal particles usually penetrate into the organic layer to induce a metal/OSC blended layer due to the high kinetic energy of the deposited metal atoms [26]. Obviously, the metal/OSC contact area is greatly enhanced in this blended layer, and the area of the reverse barrier is also remarkably increased. As a result, the blended layer has high conductivity and the resistivity of the whole Co/P3HT film decreases. It is noteworthy that the above discussion of charge transfer is based on the metal/inorganic semiconductor contact model, which has also been used for some other metal/organic semiconductor systems [27,28]. In a real metal/OSC system, the work function of metal will be affected by the push-back effect and the interface ionization potential of the organic materials, making the mechanism more complicated [29–31].

Room-temperature (RT) MR curves of bare Co films changing from 10 to 50 nm thickness are shown in Fig. 3(a). Here, the MR is defined as

$$\text{MR} = \frac{[R(H) - R(0)]}{R(0)}, \quad (1)$$

where $R(H)$ and $R(0)$ represent the resistances measured under a certain magnetic field and without a magnetic field, respectively. The applied magnetic field is perpendicular to the film. All the bare Co films show negative MRs with similar values independent of the film thickness. The resistance does not saturate in the applied magnetic field range of ±1.5 T. In the inset of Fig. 3(a), the MR curves of the Co_10 film are measured in the magnetic field parallel to the electric current (∥) or perpendicular to the surface of the film (⊥), respectively. The resistance decreases more rapidly with a lower saturation field of about 0.8 T when the magnetic field is parallel to the current.

The most familiar MR effect in Co film is the anisotropic magnetoresistance (AMR) effect, which comes from the *s-d* scattering and the SOC [32]. Generally, in a metallic sample, the relative orientation between the electric current

and magnetization varies the scattering cross section of the conduction electrons, thus the resistivity strongly depends on the orientation between electric current (I) and magnetic field (H). If I is parallel to H, MR is positive, while if I is perpendicular to H, MR is negative [33,34]. However, in this work, even if I is parallel to H, the MR is still negative (also shown in Fig. S3 in the Supplemental Material [18]), which is distinct from AMR. The absence of AMR can be reasonably explained. As discussed in above, the Co film is composed of disordered nanosized granules. A large number of Co granule boundaries significantly scatter the conduction electrons and this type of boundary scattering is independent of the magnetic field direction. These features lead to the conduction mechanism deviating from the metallic conductivity of the Co film, confirmed by the high resistivity of up to three orders larger than that of the normal Co film. Considering the conduction network as a series of internal resistances of the Co grains and the boundary resistances, since the boundary resistance is much larger than the internal resistance [35,36], a small change in the grain internal resistance in the magnetic field, that is, the AMR, will not yield a significant impact on the total resistance.

Although MR has little relationship with the relative orientations of I and H, it has an obvious correlation with magnetization. As shown in Figs. S3 and S4 (see Supplemental Material [18]), when H is in-plane, the magnetization is easy to saturate because of the easy axis in the plane and MR is saturated rapidly. In contrast, when H is out-of-plane, the magnetization is hard to saturate and MR is saturated slowly. In addition, the saturation value of MR has no evident difference for different in-plane H directions. These behaviors are similar to the giant magnetoresistance (GMR) effect [37], but the values of MR are much smaller than GMR. The same effects have also been found in other hybrid granular or polycrystalline systems, such as $Co_{70}Fe_{30}$/GeTe and $Co_{70}Fe_{30}$/$Ge_2Sb_2Te_5$ granular films [37], granular Fe-Al-O films [38], polycrystalline Fe_3O_4 films [39], polycrystalline $Ti_{1-x}Cr_xN$ films [40], and so on.

The origin of this kind of small negative MR is the spin-dependent scattering due to the existence of granules [36].

The spin-polarized carriers are transported through a network of contiguous granules and the grain boundary serves as the pinning center and contributes to the MR [37]. This mechanism can be proved by the fitting of MR $\sim (M/M_s)$ curves, where M and M_s represent magnetization and saturated magnetization, respectively. The results are shown in Fig. S5 (see Supplemental Material [18]). It can be observed that the curves fit well with the function of MR $= a(M/M_s)^2 + b(M/M_s)^4$, indicating that the MR effect here depends on the grain boundary scattering of magnetic grains with strong coupling between grains [41]. The not well-defined boundaries could be responsible for the relatively small MR effect [37].

In contrast to the Co films, the Co/P3HT hybrid films show totally different MR curves at RT, as shown in Fig. 3(b). In the low perpendicular magnetic field below 0.5 T, the resistance of Co/P3HT films increases with the increasing magnetic field, which is contrary to the bare Co samples. As the magnetic field continues increasing, the resistance reaches a maximum and starts to decrease. The overall MR of Co/P3HT shows a crossover behavior between positive and negative. With the Co thickness decreasing, the positive MR gradually dominates the MR of Co/P3HT.

In order to reveal the origin of this MR crossover phenomenon, the MR of the Co_10/P3HT sample is also measured in the parallel magnetic field direction as presented in the inset of Fig. 3(b). It shows that when the magnetic field is parallel to the current, the MR is negative, similar to that of the Co_10 film in a parallel magnetic field. This means that the positive MR can only appear in the perpendicular magnetic field, which strongly suggests that the positive MR in the Co/P3HT films derives from the Lorentz force. In the Co/P3HT films, the carriers accumulate in the reverse barrier layer. When the applied magnetic field is perpendicular to the film, these moving carriers will apparently be influenced by Lorentz force and show cyclotron motion. This will enhance the scattering probability and improve the resistivity. Especially in a metal/organic hybrid structure, the Co particles more easily penetrate into the P3HT matrix and form the Co/P3HT

blended layer during the sputtering process due to the soft texture of P3HT [13,26]. This increases the thickness of the reverse barrier layer and accordingly, the number of the carriers. As a result, the Lorentz force-induced positive MR is more remarkable than that of the bare Co sample. In the parallel case, the conduction of the carriers is not affected by the Lorentz force, so the MR of Co/P3HT retains the same trend as the bare Co samples. Clearly, the observed MR behavior at RT in the perpendicular magnetic field is the result of the competition between the negative MR of Co and the positive MR induced by the Lorentz force. The schematic diagram is summarized in Fig. S6 (see Supplemental Material [18]). Additionally, the influences of Hall effect, the surface oxidation layer of Co, and the pure P3HT layer have also been excluded. The relative discussion and figures are shown in Sec. 7 in Supplemental Material [18].

In this work, the Co granules penetrate into P3HT forming the metal/organic hybrid interface, which induces the MR crossover phenomenon. It is noteworthy that the directivity of this hybrid interface is rather weak due to the granularity of Co. This type of interface effect can exist even if the current is out-of-plane in a general OSV device.

The variable temperature MR of Co_10 in a ± 5 T perpendicular magnetic field is presented in Fig. 4(a). The MR value decreases from 300 to 100 K and then increases below approximately 50 K, which is in accordance with the T_{min} (approximately 83 K) shown in Fig. 2(a). However, the Co_50 film shows the opposite trend, as shown in Fig. 4(b). Obviously, there are two different mechanisms that dominate the magneto-transport at the two sides of T_{min} for Co_10.

It has been reported that both the electron-electron interaction (EEI) and the WL effect will lead to a resistivity increase and $\rho - \log T$ linear dependence at low temperature [42], thus the electric transport analysis alone cannot distinguish WL from EEI. In WL-dominated systems, even a small magnetic field can destroy the spin coherence of electrons. To confirm the existence of WL at low temperature in Co_10, the variation of conductivity over one decade of temperature under different perpendicular
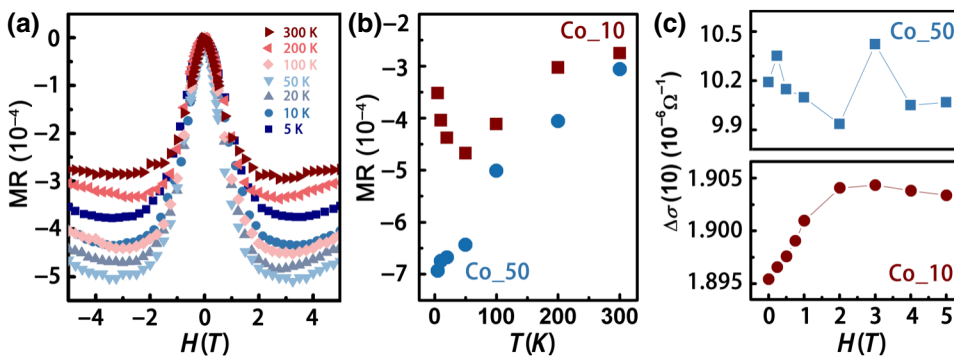

FIG. 4. (a) Variable temperature MR curves of Co_10 in the perpendicular magnetic field, (b) the MR values in different temperatures of Co_10 and Co_50, and (c) conductivity variation $\Delta\sigma$ under 10 K curves vs magnetic field for Co_50 and Co_10 samples.

magnetic fields is measured and the variation $\Delta\sigma(T)$ is characterized by [21]

$$\Delta\sigma(T) = \frac{R_S(T^*) - R_S(T)}{R_S^2(T)}, \qquad (2)$$

where $R_S(T)$ is the sheet resistance at temperature T, and $R_S(T^*)$ is the sheet resistance at 2 K. The $\Delta\sigma(10)$ vs magnetic field curves of Co_10 and Co_50 are presented in Fig. 4(c). The $\Delta\sigma(10)$ of Co_50 is clearly independent of the applied magnetic field, while the $\Delta\sigma(10)$ of Co_10 is field dependent and increases continuously until 2 T, then remains stable at the higher magnetic field. This result together with the former analysis of electric transport confirms the existence of WL in Co_10. In this Co-CoO system with strong spin-dependent scattering, a perpendicular magnetic field will destroy the spin coherence of the electrons and lead to the resistance increase with magnetic field, that is, the MR increases (the value of the negative MR decreases) at low temperature. Therefore, the decrease of the MR value below $T_{\min}$ may come from the WL effect. In contrast, for the Co_50 sample without the WL effect, the MR decreases monotonically with decreasing temperature as shown in Fig. S8 (see Supplemental Material [18]).

Figure S9 (see Supplemental Material [18]) shows the variable temperature MR curves of Co_10/P3HT measured in a perpendicular magnetic field. The resistance increases rapidly at the low-field region and then decreases until about 2 T, which corresponds to the saturated field of bare Co film as shown in Fig. 4(a). When the field is higher than 2 T, the Lorentz force-caused positive MR becomes dominant. Therefore, the overall variation trend is the result of the superposed MR in Co film and the Co/P3HT interface. In addition, it can be seen that the MR of Co_10/P3HT monotonically decreases with decreasing temperature, indicating that the negative MR becomes more and more pronounced with decreasing temperature.

IV. CONCLUSION

In summary, the WL effect emerges in the Co films with a slightly surface-oxidized CoO phase. This will lead to increased resistivity and decreased MR at low temperature. In the presence of P3HT, the MR is reversed from negative to positive in Co/P3HT hybrid films due to the competition between two mechanisms: the negative MR is the result of spin-dependent scattering and the positive MR is caused by the Co/P3HT contact effect. The carriers in the high electric conductivity Co/P3HT contact area conduct cyclotron motion due to the Lorentz force and have a higher scattering probability in the perpendicular magnetic field. In the OSV devices, the interface plays an important role in improving the MR value at room temperature, so the properties of the interface should be thoroughly understood.

This experiment extracts this interface. The observed MR crossover phenomenon clearly shows the existence of this interfacial layer and its obvious influence, which should be given full attention in actual organic devices, especially when the total MR is small.

[1] T. N. Ng, W. S. Wong, M. L. Chabinyc, S. Sambandan, and R. A. Street, Flexible image sensor array with bulk heterojunction organic photodiode, Appl. Phys. Lett. **92,** 213303 (2008).

[2] E. Arisi, I. Bergenti, V. Dediu, M. A. Loi, M. Muccini, M. Murgia, G. Ruani, C. Taliani, and R. Zamboni, Organic light emitting diodes with spin polarized electrodes, J. Appl. Phys. **93,** 7682 (2003).

[3] B. Blülle, R. Häusermann, and B. Batlogg, Approaching the Trap-Free Limit in Organic Single-Crystal Field-Effect Transistors, Phys. Rev. Appl. **1,** 034006 (2014).

[4] N. Sergeeva, S. Ullbrich, A. Hofacker, C. Koerner, and K. Leo, Structural Defects in Donor-Acceptor Blends: Influence on the Performance of Organic Solar Cells, Phys. Rev. Appl. **9,** 024039 (2018).

[5] D. W. Shao, Y. H. Cheng, J. He, D. Q. Feng, L. C. Zheng, L. J. Zheng, X. H. Zhang, J. P. Xu, W. C. Wang, W. H. Wang, F. Lu, H. Dong, L. Y. Li, H. Liu, R. K. Zheng, and H. Liu, A spatially separated organic-inorganic hybrid photoelectrochemical cell for unassisted overall water splitting, ACS Catal. **7,** 5308 (2017).

[6] V. Dediu, M. Murgia, F. C. Matacotta, C. Taliani, and S. Barbanera, Room temperature spin polarized injection in organic semiconductor, Solid State Commun. **122,** 181 (2002).

[7] X. N. Sun, S. Velez, A. Atxabal, A. Bedoya-Pinto, S. Parui, X. W. Zhu, R. Llopis, F. Casanova, and L. E. Hueso, A molecular spin-photovoltaic device, Science **357,** 677 (2017).

[8] M. N. Baibich, J. M. Broto, A. Fert, F. Nguyen Van Dau, F. Petroff, P. Eitenne, G. Creuzet, A. Friederich, and J. Chazelas, Giant Magnetoresistance of (001)Fe/(001)Cr Magnetic Superlattices, Phys. Rev. Lett. **61,** 2472 (1988).

[9] D. L. Sun, E. Ehrenfreund, and Z. V. Vardeny, The first decade of organic spintronics research, Chem. Commun. **50,** 1781 (2014).

[10] C. Barraud, P. Seneor, R. Mattana, S. Fusil, K. Bouzehouane, C. Deranlot, P. Graziosi, L. Hueso, I. Bergenti, V. Dediu, F. Petroff, and A. Fert, Unravelling the role of the interface for spin injection into organic semiconductors, Nat. Phys. **6,** 615 (2010).

[11] D. Ciudad, M. Gobbi, C. J. Kinane, M. Eich, J. S. Moodera, and L. E. Hueso, Sign control of magnetoresistance

through chemically engineered interfaces, Adv. Mater. **26,** 7561 (2014).

[12] S. Mandal and R. Pati, What determines the sign reversal of magnetoresistance in a molecular tunnel junction?, ACS Nano **6,** 3580 (2012).

[13] S. S. Ding, Y. Tian, Y. Li, W. B. Mi, H. L. Dong, X. T. Zhang, W. P. Hu, and D. B. Zhu, Inverse magnetoresistance in polymer spin valves, ACS Appl. Mater. Interfaces **9,** 15644 (2017).

[14] Y. H. Zheng and F. Wudl, Organic spin transporting materials: present and Future, J. Mater. Chem. A **2,** 48 (2014).

[15] S. Wang, M. J. Ha, M. Manno, C. D. Frisbie, and C. Leighton, Hopping transport and the Hall effect near the insulator-metal transition in electrochemically gated poly(3-hexylthiophene) transistors, Nat. Commun. **3,** 542 (2012).

[16] T. L. Wen, D. Liu, C. K. Luscombe, and K. M. Krishnan, Granular magnetoresistance in cobalt/poly(3-hexylthiophene,2,5-diyl) hybrid thin films prepared by a wet chemical method, Appl. Phys. Lett. **95,** 082509 (2009).

[17] J. Yamamoto and Y. Furukawa, Raman study of the interaction between regioregular poly(3-hexylthiophene) (P3HT) and transition-metal oxides MoO_3, V_2O_5, and WO_3 in polymer solar cells, Chem. Phys. Lett. **644,** 267 (2016).

[18] See Supplemental Material at http://link.aps.org/supple mental/10.1103/PhysRevApplied.11.034024 for more details on the conductance circuit, HOMO level test of the P3HT film, MR curves, MH curves, the fitting of MR curves of Co film under different field directions, the schematic diagram of the MR crossover, excluding the contribution of surface oxidation and Hall effect to the positive MR, variable temperature MR curves of Co_50 and Co_10/P3HT.

[19] A. Carl, G. Dumpich, and D. Hallfarth, Magnetoresistance in thin palladium-carbon mixture films, Phys. Rev. B **39,** 915 (1989).

[20] D. L. Peng, K. Sumiyama, T. J. Konno, T. Hihara, and S. Yamamuro, Characteristic transport properties of CoO-coated monodispersive Co cluster assemblies, Phys. Rev. B **60,** 2093 (1999).

[21] M. Brands, A. Carl, and G. Dumpich, Absence of weak electron localization in ferromagnetic cobalt wires, Europhys. Lett. **68,** 268 (2004).

[22] C. R. Jiang, S. J. A. Moniz, A. Q. Wang, T. Zhang, and J. W. Tang, Photoelectrochemical devices for solar water splitting-materials and challenges, Chem. Soc. Rev. **46,** 4645 (2017).

[23] L. J. Brillson, The structure and properties of metal-semiconductor interfaces, Surf. Sci. Rep. **2,** 123 (1982).

[24] F. Cardon and W. P. Gomes, On the determination of the flat-band potential of a semiconductor in contact with a metal or an electrolyte from the Mott-Schottky plot, J. Phys. D: Appl. Phys. **11,** L63 (1978).

[25] T.-S. Chao, S. Member, Y.-J. Lee, and T.-Y. Huang, High-voltage and high-temperature applications of DTMOS with reverse Schottky barrier on substrate contacts, IEEE Electron Device Lett. **25,** 86 (2004).

[26] H. Vinzelberg, J. Schumann, D. Elefant, R. B. Gangineni, J. Thomas, and B. Büchner, Low temperature tunneling magnetoresistance on junctions with organic spacer layers, J. Appl. Phys. **103,** 093720 (2008).

[27] H. Ishii, K. Sugiyama, E. Ito, and K. Seki, Energy level alignment and interfacial electronic structures at organic/metal and organic/organic interfaces, Adv. Mater. **11,** 605 (1999).

[28] T. Arnold, A. Atxabal, S. Parui, L. E. Hueso, and F. Ortmann, Hot electrons and hot spins at metal-organic interfaces, Adv. Funct. Mater. **28,** 1706105 (2017).

[29] H. Fukagawa, S. Kera, T. Kataoka, S. Hosoumi, Y. Watanabe, K. Kudo, and N. Ueno, The role of the ionization potential in vacuum-level alignment at organic semiconductor interfaces, Adv. Mater. **19,** 665 (2007).

[30] M. Hollerer, D. Lüftner, P. Hurdax, T. Ules, S. Soubatch, F. S. Tautz, G. Koller, P. Puschnig, M. Sterrer, and M. G. Ramsey, Charge transfer and orbital level alignment at inorganic/organic interfaces: the role of dielectric interlayers, ACS Nano **11,** 6252 (2017).

[31] L. Romaner, G. Heimel, J.-L. Brédas, A. Gerlach, F. Schreiber, R. L. Johnson, J. Zegenhagen, S. Duhm, N. Koch, and E. Zojer, Impact of Bidirectional Charge Transfer and Molecular Distortions on the Electronic Structure of a Metal-Organic Interface, Phys. Rev. Lett. **99,** 256801 (2007).

[32] T. R. McGuire and R. I. Potter, Anisotropic magnetoresistance in ferromagnetic 3d alloys, IEEE Trans. Magn. **11,** 1018 (1975).

[33] A. Bose, H. Singh, V. K. Kushwaha, S. Bhuktare, S. Dutta, and A. A. Tulapurkar, Sign Reversal of Fieldlike Spin-Orbit Torque in an Ultrathin Cr/Ni Bilayer, Phys. Rev. Appl. **9,** 014022 (2018).

[34] B. Leven and G. Dumpich, Resistance behavior and magnetization reversal analysis of individual Co nanowires, Phys. Rev. B **71,** 064411 (2005).

[35] W. B. Mi, J. J. Shen, E. Y. Jiang, and H. L. Bai, Microstructure, magnetic and magneto–transport properties of polycrystalline Fe_3O_4 films, Acta Mater. **55,** 1919 (2007).

[36] M. Yu, H. Qiu, X. Chen, and H. Liu, Magnetic, magnetoresistance and electrical transport properties of Ni and Al co-doped ZnO films grown on glass substrates by direct current magnetron co-sputtering, Mater. Chem. Phys. **120,** 571 (2010).

[37] J. C. Huang, W. D. Song, J. A. Bain, Y. Yang, L. P. Shi, T. E. Schlesinger, T. C. Chong, and H. K. Hui, Magnetoresistance in granular films formed by CoFe and phase change material, Appl. Phys. A **113,** 221 (2013).

[38] S. Nakamura, T. Nojima, A. Yoshihara, S. Ohnuma, and H. Fujimori, Electrical resistivity in ferromagnetic TM-Al-O (TM = Fe, Co) granular films: scattering by spin waves and Kondo like behavior, J. Phys. Soc. Jpn **78,** 074708 (2009).

[39] J. M. D. Coey, A. E. Berkowitz, L. Balcelles, F. F. Putris, and F. T. Parker, Magnetoresistance of magnetite, Appl. Phys. Lett. **72,** 734 (1998).

[40] X. F. Duan, W. B. Mi, Z. B. Guo, and H. L. Bai, Magnetoresistance and anomalous Hall effect of reactive sputtered polycrystalline $Ti_{1-x}Cr_xN$ films, Thin Solid Films **542,** 348 (2013).

[41] G. Zhang, C. Fan, L. Pan, F. Wang, P. Wu, H. Qiu, Y. Gu, and Y. Zhang, Magnetic and transport properties of magnetite thin films, J. Magn. Magn. Mater. **293,** 737 (2005).

[42] G. Bergmann, Quantitative analysis of weak localization in thin Mg films by magnetoresistance measurements, Phys. Rev. B **25,** 2937 (1982).